International Journal of Nanomedicine

Dovepress
open access to scientific and medical research

Open Access Full Text Article

ORIGINAL RESEARCH

Gold nanorods/mesoporous silica-based nanocomposite as theranostic agents for targeting near-infrared imaging and photothermal therapy induced with laser

This article was published in the following Dove Press journal:
International Journal of Nanomedicine
28 July 2015
Number of times this article has been viewed

Yang Liu[1,2]
Ming Xu[3]
Qing Chen[1]
Guannan Guan[1]
Wen Hu[3]
Xiuli Zhao[1]
Mingxi Qiao[1]
Haiyang Hu[1]
Ying Liang[2]
Heyun Zhu[1]
Dawei Chen[1]

[1]School of Pharmacy, Shenyang Pharmaceutical University, Shenyang, [2]Department of Pharmacy, Bengbu Medical College, Bengbu, [3]College of Pharmaceutical Science, Soochow University, Suzhou, People's Republic of China

Abstract: Photothermal therapy (PTT) is widely regarded as a promising technology for cancer treatment. Gold nanorods (GNRs), as excellent PTT agent candidates, have shown high-performance photothermal conversion ability under laser irradiation, yet two major obstacles to their clinical application are the lack of selective accumulation in the target site following systemic administration and the greatly reduced photothermal conversion efficiency caused by self-aggregating in aqueous environment. Herein, we demonstrate that tLyp-1 peptide-functionalized, indocyanine green (ICG)-containing mesoporous silica-coated GNRs (I-TMSG) possessed dual-function as tumor cells-targeting near-infrared (NIR) fluorescent probe and PTT agents. The construction of the nanostructure began with synthesis of GNRs by seed-mediated growth method, followed by the coating of mesoporous silica, the chemical conjugation of PEG and tLyp-1 peptide, and the enclosure of ICG as an NIR imaging agent in the mesoporous. The as-prepared nanoparticles could shield the GNRs against their self-aggregation, improve the stability of ICG, and exhibit negligible dark cytotoxicity. More importantly, such a theranostic nanocomposite could realize the combination of GNRs-based photothermal ablation under NIR illumination, ICG-mediated fluorescent imaging, and tLyp-1-enabled more easy endocytosis into breast cancer cells. All in all, I-TMSG nanoparticles, in our opinion, possessed the strong potential to realize the effective diagnosis and PTT treatment of human mammary cancer.

Keywords: theranostic nanoagents, photothermal therapy, indocyanine green, gold nanorods, mesoporous silica, anti-mammary cancer

Introduction

Compared with traditionally used chemotherapy and radiotherapy, photothermal therapy (PTT), which generally employs PTT agents to kill cancer cells by reaching sufficient hyperthermia (>42°C) under laser irradiation, has been considered as a highly specific and minimally invasive cancer therapy.[1–7] To balance efficacy with safety concerns, an ideal photo-absorbing agent should have strong light absorbance in the near-infrared (NIR) tissue transparency window as well as high tumor-specific accumulation with minimal retention in other normal organs.[8–11] Furthermore, to judge the optimal timing of laser treatment and the highest peaked accumulation of PTT agent in the targeted niduses, imaging technologies[12,13] may be introduced to direct the design of therapy plans in bedside applications.[14–18] In order to accomplish the above purpose simultaneously through a single nanocomposite, lots of the theranostic nanosystem,[19–23] such as bovine serum albumin (BSA) protein-modified IR825-loaded

Correspondence: Dawei Chen
School of Pharmacy, Shenyang Pharmaceutical University, No 103 Wenhua Road, Shenyang, 110016, People's Republic of China
Tel +86 24 2398 6306
Fax +86 24 2398 6305
Email chendawei@syphu.edu.cn

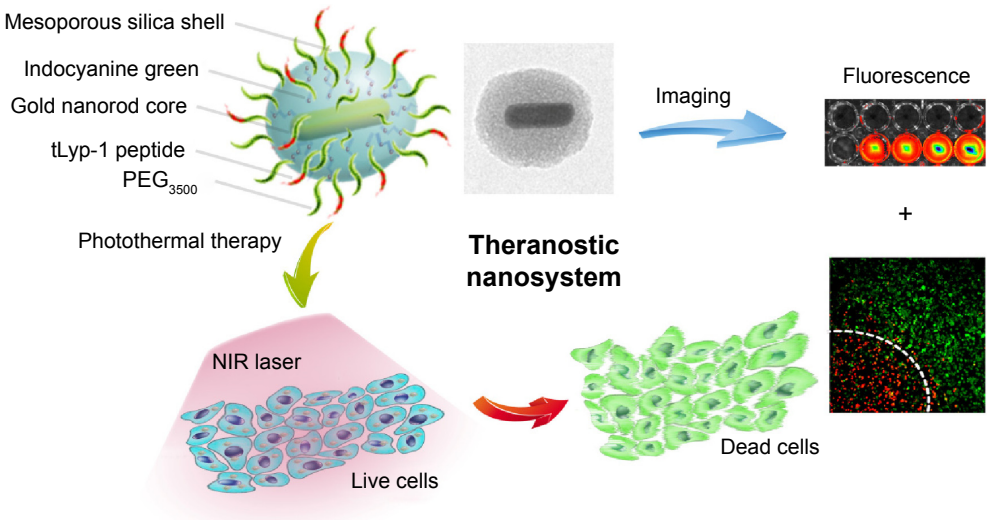

Figure 1 A schematic illustration to show the formation of I-TMSG complex, as well as its theranostic application to photothermal therapy treatment and near-infrared fluorescence imaging.
Abbreviations: I-TMSG, tLyp-1 peptide-functionalized, indocyanine green-containing mesoporous silica-coated gold nanorods; PEG_{3500}, polyethylene glycol-3500; NIR, near-infrared.

upconversion nanoparticles,[24] copper sulfide-loaded Cy5.5-conjugated hyaluronic acid nanoparticles,[25] and Cy3-attached S6 aptamer-conjugated magnetic core-plasmonic shell star shape nanoparticles,[26] which were based on the combination of PTT agents and NIR fluorescence agents have been developed and hold out encouraging treatment effects. Typically, fluorescent drug-loaded, polymeric-based, branched gold nanoshells were recently configured as multifunctional nanotheranostic platform and acted not only in a combinational fashion but also in a coordinated model in vivo to optimize therapeutic efficacy and safety of therapeutic regimes.[27]

Gold nanorods (GNRs), as excellent PTT agent candidates, have shown high-performance photothermal conversion ability in the NIR region.[28–30] Unfortunately, similar to most PTT agents, it is still a major challenge to achieve selective accumulation of GNRs in the target site after systemic administration.[31–33] What is more, the desirable NIR window of the GNRs may shift to the visible spectral region as a result of frequently observed aggregating and clustering of the GNRs within different cells, and this would greatly reduce the photothermal conversion efficiency.[34–36] Thus, a number of nanoscale encapsulation systems, including thermoresponsive polymer,[37] multidentate polyethylene glycol (PEG),[38] human serum albumin,[39] poly(amido amine[PAMAM]) dendrimer,[40] chitosan,[41] mesoporous silica,[42] and calf thymus DNA,[43] have been developed to encapsulate GNRs and show their unique and enhanced therapeutic effects by thermal ablation of tumors.

To achieve more efficient PTT and improve therapeutic selectivity, we herein reported tLyp-1 peptide-functionalized, indocyanine green (ICG)-containing mesoporous silica-coated GNRs (I-TMSG) as a novel cancer theranostic nanoagent. In such nanostructure (Figure 1), tLyp-1, a newly reported tumor-homing heptapeptide,[44] acted as a ligand selectively targeted to neuropilin protein (a membranous receptor that was overexpressed in many types of tumor cells[45]) on the cell surface and thus succeeded in achieving active targeting and ligand-mediated endocytosis. Second, mesoporous silica, a porous nanostructural biomaterial that allows for high drug loading capacity and attachment of different functional groups, was introduced to protect and shield the GNRs against their self-aggregation as well as be loaded with imaging agent and be decorated with functional peptide. Third, ICG, as a FDA-approved cyanine NIR fluorochrome,[46] was absorbed into the mesoporous as a molecular imaging probe and thus was conducive to achieving the optimized therapeutic outcome by real-time track of the PTT agent following systemic administration. These nanoagents could incorporate multiple functionalities (including imaging-guided PTT and active targeting to mammary carcinoma cells) within one nanoscaffold. Therefore, I-TMSG nanoparticles, in our opinion, possessed the strong potential to realize the effective diagnosis and PTT treatment of human mammary cancer.

Materials and methods

Materials

Chloroauric acid trihydrate ($HAuCl_4 \cdot 3H_2O$), tetraethyl orthosilicate (TEOS), and cetyltrimethylammonium bromide (CTAB) were obtained from Sinopharm Group Co. Ltd. (Shanghai, People's Republic of China). ICG was purchased

from J&K Chemical Ltd. (Shanghai, People's Republic of China). MAL-PEG$_{3500}$-NHS was provided by JenKem Technology Co., Ltd. (Beijing, People's Republic of China). tLyp-1 peptide (sequence: CGNKRTR) was custom synthesized by GL Biochem (Shanghai, People's Republic of China). Calcein-AM was purchased from Santa Cruz Biotechnology Inc. (Dallas, TX, USA). Rhodamine B isothiocyanate (RBITC) was obtained from Sigma-Aldrich Co. (St Louis, MO, USA). Annexin V-FITC/PI kit was purchased from Beyotime Institute of Biotechnology (Jiangsu, People's Republic of China). All other chemicals were of analytical or chromatographic grade and were used without further purification.

Synthesis of GNRs

The synthesis of GNRs, GNRs@mSiO$_2$ (MSG), PEG-GNRs@mSiO$_2$ (PMSG), and PEG-GNRs@mSiO$_2$-tLyp-1 (TMSG) is schematically illustrated in Figure 2. GNRs were prepared by seed-mediated growth method with minor revisions.[47] First, 600 µL of NaBH$_4$ (0.01 M) was mixed with 9.4 mL of aqueous solution containing 7.5 mL of CTAB (0.1 M) and 250 µL of HAuCl$_4$ (0.01 M). It was then kept at 30°C for 3 hours before being further used as seed solution. Second, the growth solution contained 100 mL of CTAB (0.1 M), 5 mL of HAuCl$_4$ (0.01 M), 800 µL of AgNO$_3$ (0.01 M), 2 mL of H$_2$SO$_4$ (0.5 M), and 800 µL of ascorbic acid (0.1 M). After vigorous stirring of the growth solution, 240 µL of seed solution was added and let to stew for another 15 hours at 30°C to obtain GNRs.

Synthesis of MSG

The mesoporous silica coating on bare GNRs was achieved by modified Stöber method and referred to previous reports[48] with slight modifications. Briefly, the obtained 12 mL of GNRs solution were washed with Milli-Q water twice to remove the excess CTAB and redispersed in 1 mL of water. Next, 200 µL of CTAB solution (0.2 M) was added to 1 mL of GNRs solution. After stirring for 15 minutes, 300 µL of 17% (v/v) TEOS in ethanol and 5 µL of 30% ammonia were in turn added. The silica shell could gradually form within 15 hours, and the nanoparticles were then collected by repeated centrifugation and washing with water. Furthermore, to remove the template of CTAB, the nanoparticles were dispersed in 60 mL of ethanol containing NH$_4$NO$_3$ (10 mg/mL) and were then refluxed for 10 hours at 45°C. The products were harvested by centrifugation and repeatedly washed with ethanol and water several times.

Synthesis of PMSG and TMSG

The synthesis process of TMSG consisted of three steps (Figure 2), and PEG$_{3500}$ was used as a linker to connect MSG with polypeptide (tLyp-1). First, 7 mg of MSG was dispersed in 50 mL of DMSO, and 500 µL of APTES was then added. The mixture was allowed to react for 20 hours, and then was collected by centrifugation and washed with ethanol twice. Second, amine-functionalized MSG (MSG-NH$_2$) was redispersed in 6 mL of DMSO, and 4 mg of NHS-PEG$_{3500}$-MAL was added. The mixture was then stirred at room temperature for 8 hours under anhydrous condition before collected by centrifugation. Third, the product was redispersed in DMSO, and 1.5 mg of thiol end-capped tLyp-1 peptide was then added. After 48 hours of reaction at the room temperature, 10 µL of β-mercaptoethanol was added and reacted for 1 hour at 37°C. The products were collected by repeatedly washing with distilled water several times and finally dispersed

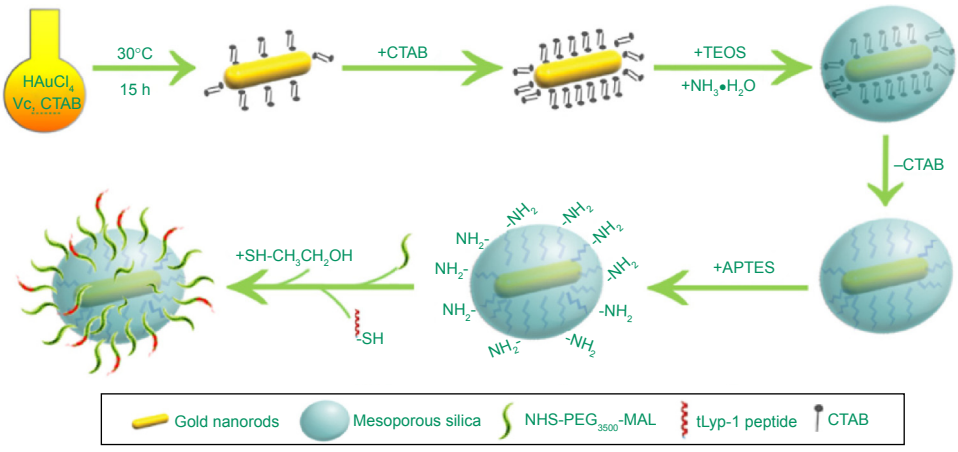

Figure 2 A schematic procedure for the preparation of TMSG nanoparticles.
Abbreviations: TMSG, tLyp-1 peptide-functionalized and polyethylene glycol-modified mesoporous silica-coated gold nanorods; APTES, aminopropyl triethoxysilane; NHS-PEG$_{3500}$-MAL maleimide PEG N-hydroxylsuccinimide ester; CTAB, cetyltrimethylammonium bromide; h, hours; TEOS, tetraethyl orthosilicate.

in water and stored at 4°C for further use. For synthesis of PMSG, the whole process was the same as that for TMSG except tLyp-1 was not added.

Characterization

The morphological examination of MSG was performed on a transmission electron microscope (TEM). The particle size distribution and zeta potential of MSG, PMSG, and TMSG were determined by size and zeta potential sizer (Nicomp 380 ZLS). For quantitative determination of Au content in MSG nanoparticles, atomic absorption spectroscopy analysis was used after the nanomaterials were digested by aqua regia. Moreover, to confirm the surface modification of TMSG and PMSG nanoparticles, bicinchoninic acid (BCA) assay, X-ray photoelectron spectroscopy (XPS), and thermogravimetric analysis (TGA) were performed. (For a detailed description of the various methods, please refer Supplementary materials).

ICG loading and optical spectra measurements

For ICG encapsulation, the TMSG or PMSG nanoparticles (1.5 mg) and ICG (150 μg) were mixed according to the mass ratio 10:1 using aqueous-based preparation method. The mixed solutions were stirred vigorously at room temperature for 3 hours in dark and then collected by repeated centrifugation and washing with water. The absorption and fluorescence spectra of I-TMSG and freely dissolved ICG (5 μg/mL) were obtained using a UV–vis spectrometer (UV-2600; Shimadzu, Japan) or fluorescence spectrometer (FM4P-TCSPC; HORIBA Jobin Yvon, France).

In vitro fluorescence imaging

In order to real-time visualize the off–on process of the fluorescence signal, MDA-MB-231 cells were preseeded in a 24-well plate (2×10^5 cells/well) and then incubated with I-TMSG for various periods (2 hours, 4 hours, 6 hours, and 8 hours). After washed, the plate was imaged by IVIS Lumina II Imaging System and the fluorescence signals of ICG (745 nm excitation) were collected. The groups treated without cells and free ICG solutions were used as control groups.

RBITC labeled the nanoparticles

To study the cellular uptake level, rhodamine-labeled TMSG (R-TMSG) or PMSG (R-PMSG) were prepared. Briefly, RBITC dye was prepared in methanol solution and then mixed with amine-functionalized MSG, reacting overnight at room temperature. The following procedure was as same as the preparation of TMSG or PMSG.

Cellular uptake analysis of TMSG nanoparticles

To directly observe the cellular uptake level, MDA-MB-231 cells were preseeded in six well plates and then incubated with R-TMSG or R-PMSG for 1 hour or 2 hours, respectively. After washing, the cells were stained with Hoechst 33342 and fixed by 4% polyoxymethylene and then imaged by a confocal laser scanning microscope (CLSM; Carl Zeiss Meditec AG, Jena, Germany). Alternatively, MDA-MB-231 cells were preseeded in six-well plates and then incubated with R-TMSG or R-PMSG for 30 minutes, 60 minutes, or 120 minutes, respectively. After washing, the cells were detached with 0.05% trypsin and harvested, followed by flow cytometric analysis (BD Biosciences FCASCalibur flow cytometer; BD Biosciences, San Jose, CA, USA). The autofluorescence of the cells was used as a control.

To further study the mechanism of cellular uptake of TMSG in MDA-MB-231 cells, cellular association of the nanoparticles was determined in the presence of various endocytosis inhibitors, including chlorpromazine (10 μg/mL), colchicines (4 μg/mL), methyl-β-cyclodextrin (5 mM), genistein (200 μM), wortmannin (50 nM), and free tLyp-1 (150 μg/mL), respectively. The cells were pretreated with these inhibitors for 30 minutes (2 hours to free tLyp-1 peptide), followed by an immediate incubation with R-TMSG for another 1 hour. The quantitative analysis was performed by flow cytometric analysis as described above.

Cell viability assay

For cell toxicity assay, MDA-MB-231 cells were seeded into 96-well cell culture plates until adherent and then incubated with various concentrations of ICG-loaded or -unloaded TMSG (or PMSG) for 48 hours. The standard CCK-8 assay was performed to determine the cell viabilities relative to control untreated cells.

Temperature measurement during NIR irradiation

A volume of 1 mL of TMSG dispersed in water with different concentrations was added to EP tubes and irradiated with a 785-nm laser. Thermographic maps and temperatures were recorded with an infrared thermal imaging camera (VarioCAM Research 270; JENOPTIK, Germany).

In vitro PTT study

For PTT, preseeded MDA-MB-231 cells (in 24-well cell culture plates) were incubated with TMSG or PMSG solution at different concentrations for 4 hours and then washed with cold phosphate-buffered saline twice. The cells were irradiated by a 785-nm laser, followed by incubation for another 8 hours (as for the control group, the cells were not exposed to NIR laser or not incubated with nanoparticles). Finally, the cells were stained with Calcein-AM and PI successively for the co-staining of live and dead cells and then taken for fluorescence imaging by using CLSM. Alternatively, MDA-MB-231 cells were seeded into 96-well cell culture plates until adherent and then incubated with various concentrations of TMSG or PMSG for 4 hours. After washing, the cells were irradiated by a 785-nm laser for different periods and cultured for another 48 hours before the CCK-8 assay. The cells not exposed to NIR laser were set as the control.

Cell apoptosis assay

The cytotoxicity of PTT was also evaluated by quantification of apoptotic or necrosis tumor cells. MDA-MB-231 cells were preseeded in 48-well cell culture plates and then treated with TMSG nanoparticles for 4 hours. After washing, the cells were irradiated with the 785-nm laser for 3 minutes or 5 minutes. Then the cells were cultured for another 8 hours, followed by double-staining with Annexin V-FITC and PI. The labeled cells were analyzed by flow cytometry using a FACSCalibur flow cytometer and FlowJo software. The cells not exposed to NIR laser were set as the control.

Results and discussion

Synthesis and characterization of the nanoparticles

By using well-known seed-mediation growth method and careful control of pH, GNRs of relatively high aspect ratio (3.50±0.37, n=25) have been produced by surfactant-directed synthesis. Then, by referring to Huang's reports[48] with slight modifications, a 17.34–32.43-nm thick mesoporous silica layer wrapped around GNRs was formed via sol–gel reaction based on the hydrolysis of TEOS. By atomic absorption spectroscopy assay, the Au contents in MSG nanoparticles were 42.92%±1.32% (n=3). The GNRs, as shown in the TEM images (Figure 3A), were rodlike, and the width and length were 47.23±4.92 nm and 13.56±1.48 nm (n=25), respectively. However, the MSG nanoparticles were generally spherical in shape with good monodispersity (Figures 3B and 4A). The widely distributed mesoporous of MSG, which acted as drug or imaging-agent cargo-space, could even be observed from the high-resolution TEM images (Figure 3C).

The UV–vis spectra (Figure 3D) clearly show that the optical properties of the GNRs were altered during the forming of silicon layers. GNRs that we synthesized had a strong longitudinal surface plasmon resonance peak approxiamtely 754 nm. However, due to both the increase in the refractive index of surrounding medium and the changes in nanoparticles geometric, the longitudinal surface plasmon resonance peak exhibited a red-shift after silica coating. By nitrogen adsorption/desorption analysis, the MSG nanoparticles had a BET surface area of 509.88 m^2/g and a BJH pore diameter of 2.59 nm. The typical IV isotherm (Figure 3E) and a sharp peak of the pore size distribution (Figure 3F) indicated the characteristic of mesoporous materials and uniform mesoporous, respectively. Altogether, uniform particle sizes with controllable well-defined mesoporous structures and high specific surface area illustrated that such nanostructures could be a promising candidate of high-performance drug delivery carrier.

To avoid reticuloendothelial uptake and achieve active targeting to tumor tissues, TMSG, which were functionalized-MSG with PEG and tLyp-1 peptide, was engineered via EDC/NHS reaction. According to zeta potential (ζ) measurement, the corresponding data value of GNRs (CTAB-stabilized), MSG, MSG-NH_2, PMSG, and TMSG in ultra pure water were 31.17±1.05 mV, –21.70±2.11 mV, 14.22±1.76 mV, 1.24±0.50 mV, and 1.38±0.68 mV (n=3, Figure 4B), respectively. These results illustrated that various functional groups on the nanoparticles surface exhibited different surface-charge properties. XPS, an advanced surface chemical analysis technique, was performed, and it verified that there were N and C elements on the surface of TMSG, which were resourced from tLyp-1 peptide and PEG, respectively. But such elements were not found in MSG (Figure 4C). It is worth noting that there does not exist any Au peak (at approxiamtely 83.8–86.6 eV) in the spectra, and this further indicated that GNRs were completely embed in silica. BCA assay, an effectiveness protein detection method, also confirmed that protein was contained as a constituent in TMSG. Moreover, TGA assay, a thermal analysis method, shows that the weight loss in the thermal decomposition of TMSG and PMSG was more obvious compared with MSG (Figure 4D). These dissimilarities were ascribed to disparate thermal stability among polypeptide, hydrocarbon, and inorganic silicon compounds. Altogether, all these results strongly proved that we successfully synthesized TMSG and PMSG by MSG nanoparticles.

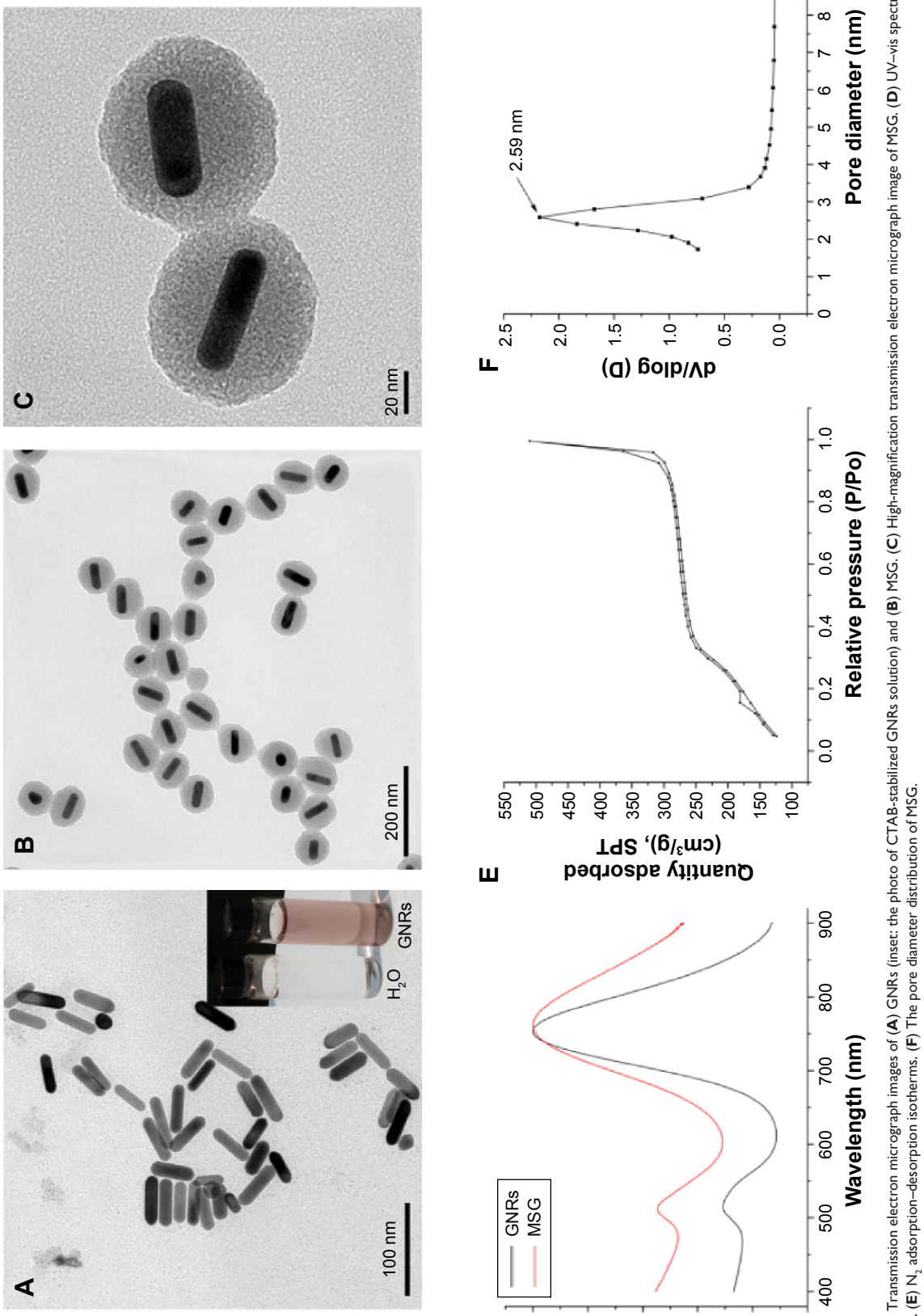

Figure 3 Transmission electron micrograph images of (**A**) GNRs (inset: the photo of CTAB-stabilized GNRs solution) and (**B**) MSG. (**C**) High-magnification transmission electron micrograph image of MSG. (**D**) UV–vis spectra of GNRs and MSG. (**E**) N_2 adsorption–desorption isotherms. (**F**) The pore diameter distribution of MSG.
Abbreviations: GNRs, gold nanorods; CTAB, cetyltrimethylammonium bromide; MSG, mesoporous silica-coated GNRs; UV, ultraviolet; SPT, standard pressure and temperature.

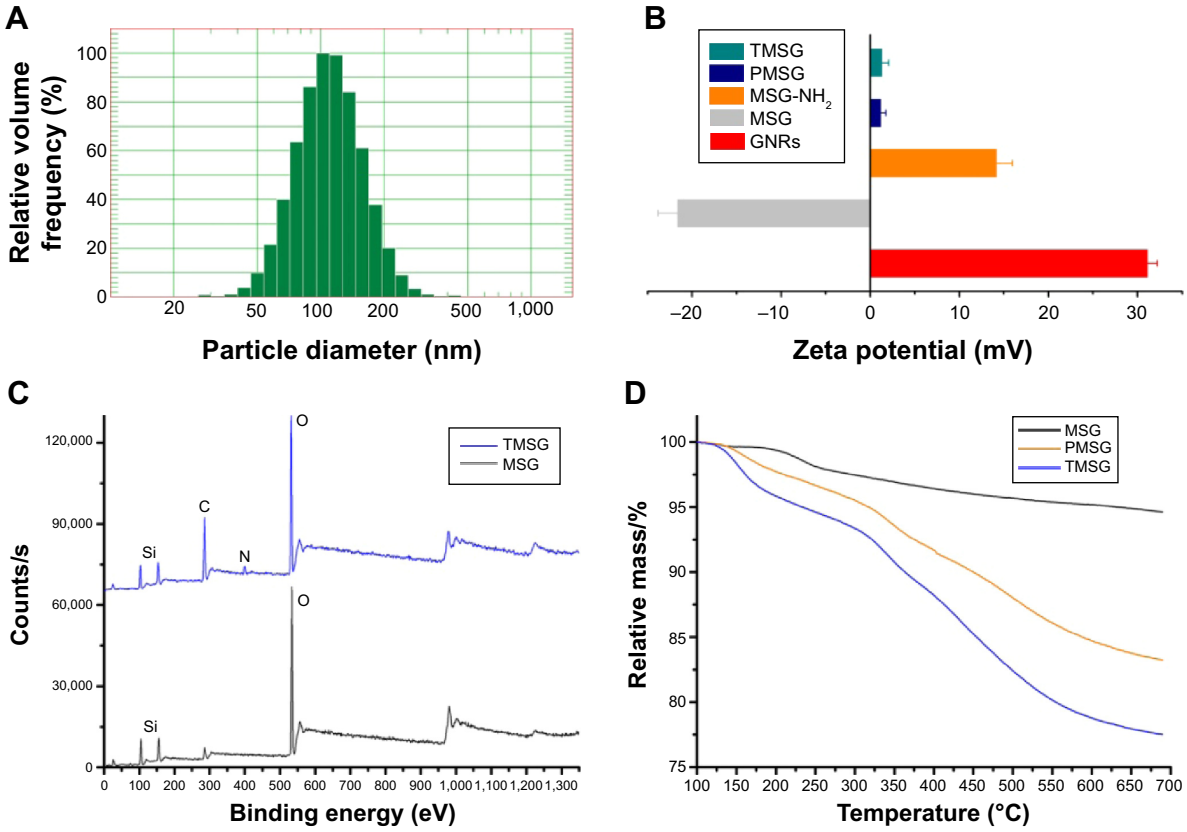

Figure 4 (**A**) Dynamic light scattering size of MSG. (**B**) Zeta potential of GNRs (CTAB stabilized), MSG, MSG-NH_2, PMSG, and TMSG (n=3). (**C**) X-ray photoelectron spectra of MSG and TMSG. (**D**) TGA curves of MSG, PMSG, and TMSG.
Abbreviations: MSG, mesoporous silica-coated GNRs; GNRs, gold nanorods; CTAB, cetyltrimethylammonium bromide; MSG-NH_2, amine-functionalized MSG; PMSG, polyethylene glycol-modified MSG; TMSG, tLyp-1 peptide-functionalized PMSG; s, second; TGA, thermogravimetric analysis.

ICG loading and characterization of the optical properties

ICG, as a safe and vigorous NIR light absorber, has been approved by FDA as a clinical imaging agent.[42] However, several drawbacks, including poor aqueous stability, concentration-dependent aggregation, and nonspecific binding to proteins, greatly limited its applications as an NIR fluorescent probe. The absorption and fluorescence spectra of free ICG and ICG-encapsulated TMSG are shown in Figure 5. Compared with TMSG, the I-TMSG exhibited broad adsorption peak ranging from 650 nm to 900 nm. However, followed by heating for 5 minutes in a water bath at 90°C, a new sharp peak at 780 nm appeared in the absorption spectra of I-TMSG, which indicated an accelerated release of ICG molecules from mesoporous with rising temperature (Figure 5A). In addition, the UV–vis spectra also show that the strong characteristic peak of free ICG nearly disappeared within 1 week, and this indicated the degradation of ICG molecules (Figure 5B). However, in the spectra of I-TMSG appeared relatively little changes, and the peak value of the absorption coefficient still retained over 90% and 80% of the original value within 1 day and 1 week, respectively (Figure 5C). These indicated that owing to being entrapped inside the nanochannels and isolated from the surrounding environment, ICG could be well protected against photodegradation and detrimental oxidation and could show significantly improved stability.

Typically, the self-aggregates of ICG that are driven by intermolecular forces, including van der Waals forces and hydrophobic interactions, would result in fluorescence quenching and may greatly reduce the effectiveness of ICG as a fluorescent tracer.[49] Not surprisingly, owing to the fluorescence quenching of ICG encapsulated intensively in the mesoporous of TMSG, there was very low fluorescence signal captured by the fluorescence spectrophotometer, which was in sharp contrast with the ICG solutions (Figure 5D). However, NIR fluorescent signals of I-TMSG could be activated in an intracellular environment in vitro. As shown in Figure 6, the fluorescence intensity of I-TMSG incubated with MDA-MB-231 cells appeared to be getting stronger within 8 hours. Obviously, owing to the accelerated release of ICG molecules from the mesoporous, the fluorescence

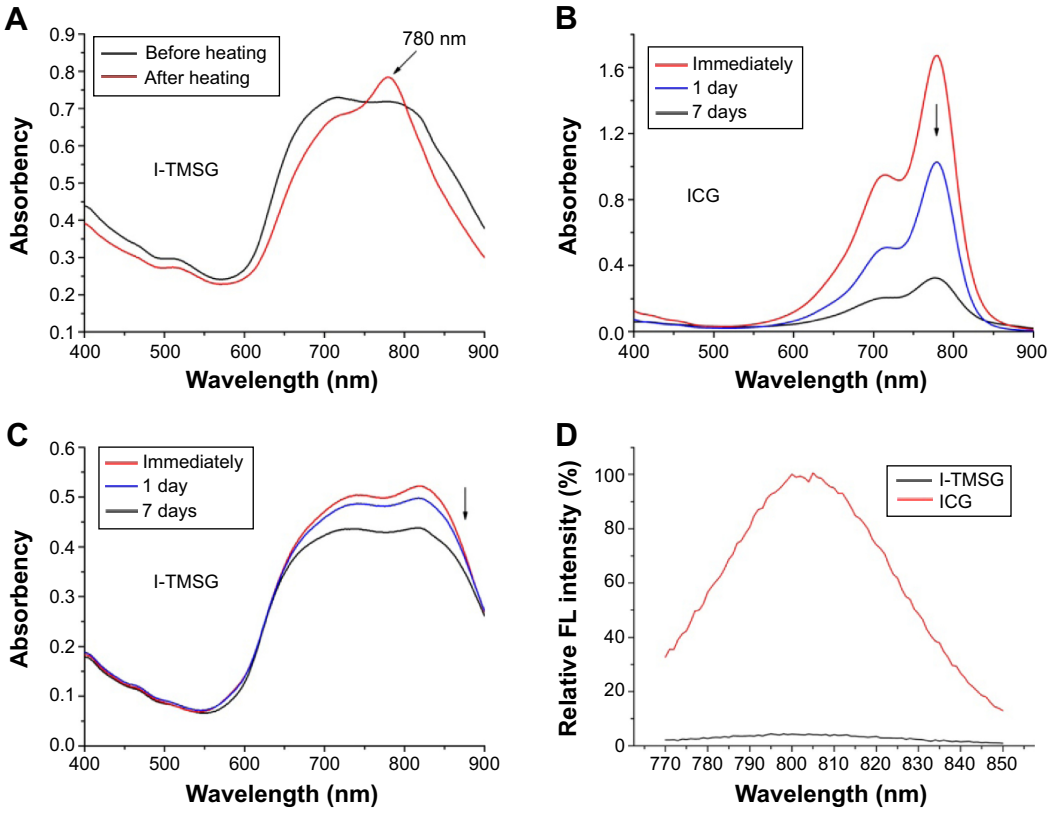

Figure 5 The UV–vis (**A**–**C**) or FL (**D**) spectra of I-TMSG and ICG solutions at different points.
Note: The results demonstrated that the probe had a high stability compared to freely dissolved ICG and the fluorescence quenching of ICG encapsulated intensively in the mesoporous of TMSG.
Abbreviations: UV, ultraviolet; FL, fluorescence; I-TMSG, tLyp-1 peptide-functionalized, indocyanine green-containing mesoporous silica-coated gold nanorods; ICG, indocyanine green.

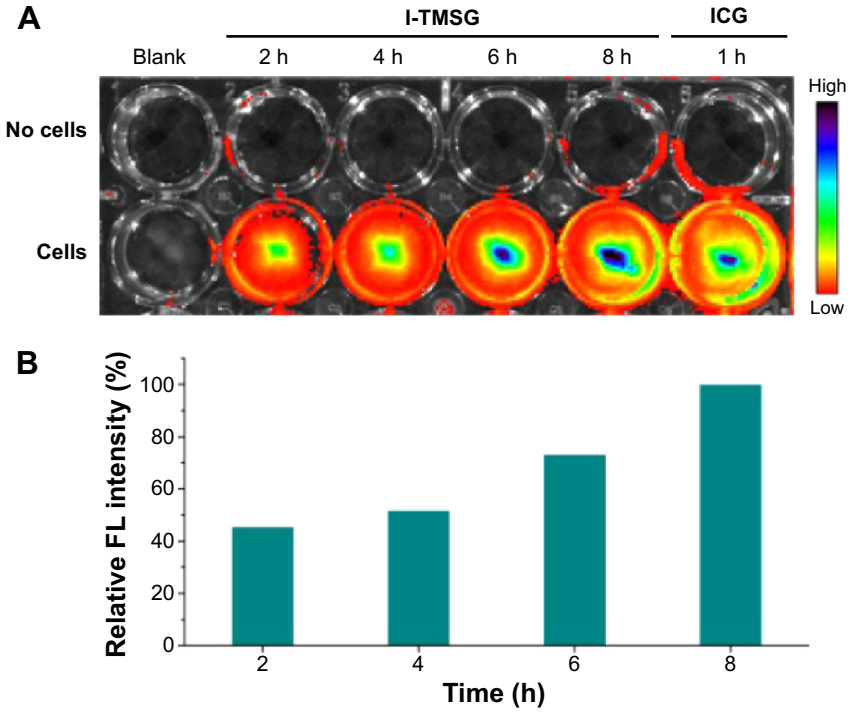

Figure 6 (**A**) The FL image and (**B**) relative FL intensity of I-TMSG nanoparticles or free ICG in culture medium coincubated with MDA-MB-231 cells or without cells at different points in time, respectively.
Abbreviations: FL, fluorescence; I-TMSG, tLyp-1 peptide-functionalized, indocyanine green-containing mesoporous silica-coated gold nanorods; ICG, indocyanine green; MDA-MB-231 cells, MD Anderson-metastatic breast-231 cells; h, hours.

of nanoparticles could be activated from off to on in the cytoplasm of tumor cells.

Targeting uptaking of TMSG by tumor cells

tLyp-1, similar to extensively studied iRGD and RGD, is a tumor-homing peptide first reported in 2012.[44] Recently, tLyp-1-conjugated iron oxide nanoparticles,[44] PEG-PLA (polyethylene glycol–polylactic acid) nanoparticles,[50] and cationic liposomes[51] were constructed by different groups and showed robust and selective homing to tumors, penetrating from the blood vessels into the tumor parenchyma. To examine the characteristics of TMSG as a targeting nanoparticle to human breast cancer MDA-MB-231 cells, optical imaging experiments about endocytosis of fluorescent-labeled nanoparticles were performed. As shown in Figure 7, compared with TMSG, PMSG presented the relatively low intracellular nanoparticle concentrations (represented by red fluorescence). Such results were further demonstrated by fluorescence histograms obtained by flow cytometric analysis (Figure 8A). The mean fluorescence intensity of intracellular TMSG was 1.44-fold higher than that of PMSG ($P<0.001$, n=3). These results illustrated that TMSG, as a targeting nanomaterial, although contained sterically hindered PEG chains wrapped around the nanoparticles, still shows quite high endocytosis rate, and such phenomenon indicated that there might have been direct crosstalking between tLyp-1-decorated nanoparticles and the corresponding cell surface receptor. To test this hypothesis, we further explored the endocytic pathway of TMSG through coincubating the cancer cells with different competitive or uncompetitive endocytosis inhibitors. As shown in Figure 8B, preincubation with chlorpromazine (clathrin-mediated endocytosis inhibitor), methyl-β-cyclodextrin (lipid raft inhibitor), and free tLyp-1 peptides (competitive inhibitor) significantly decreased the internalization of TMSG by 26.9% ($P<0.001$), 18.7% ($P<0.05$), and 30.4% ($P<0.001$), respectively. Such results indicated that the cellular uptake of TMSG in MDA-MB-231 cells was a clathrin/lipid raft-mediated endocytosis. In addition, preincubating tLyp-1 peptide, which might have occupied the same regions of neuropilin protein (the ligand of tLyp-1 peptide) on cell surface, could effectively inhibit TMSG into the cytoplasm, and this further confirmed the important role of tLyp-1 in nanoparticles endocytosis.

Enhanced killing of cancer cells with targeting TMSG nanoparticles

Before conducting PTT experiments, we first assessed in vitro dark cytotoxicity of TMSG and PMSG by the cell viability assay.

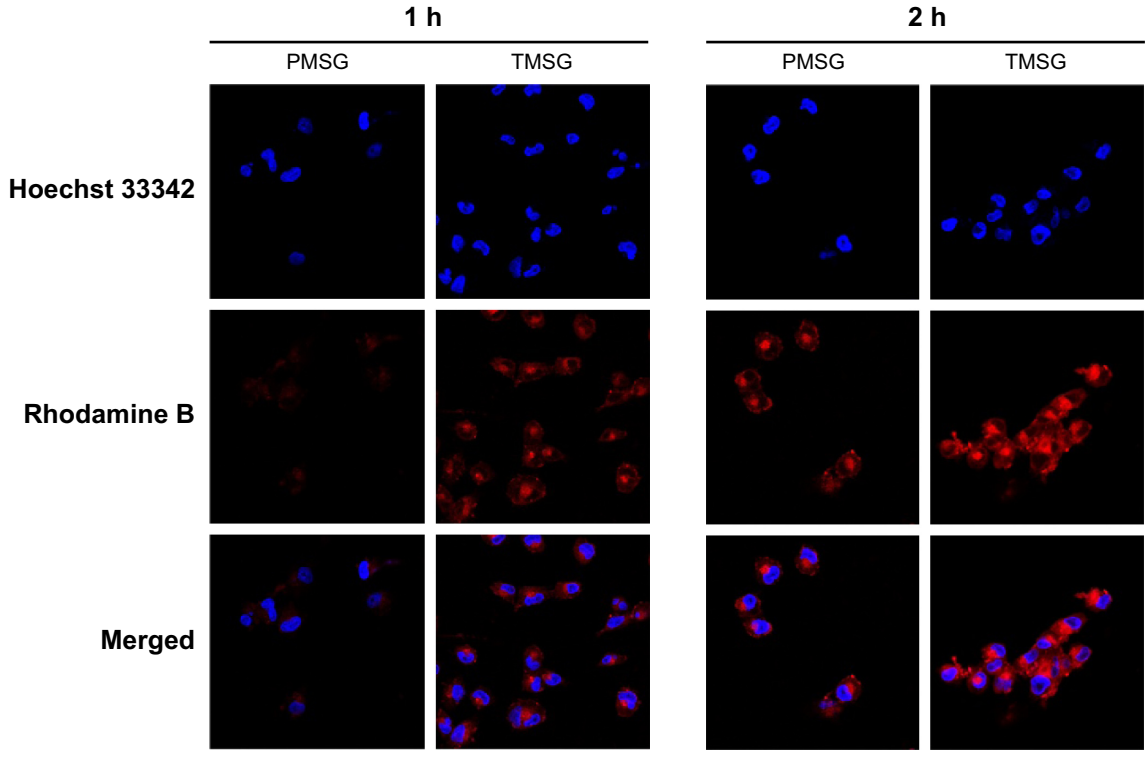

Figure 7 Confocal laser scanning microscope images of MDA-MB-231 cells incubated with rhodamine-labeled PMSG or TMSG. Blue: Hoechst 33342 and red: rhodamine B.

Abbreviations: PMSG, polyethylene glycol-modified mesoporous silica-coated gold nanorods; TMSG, tLyp-1 peptide-functionalized PMSG; h, hours; MDA-MB-231cells, MD Anderson-metastatic breast-231 cells.

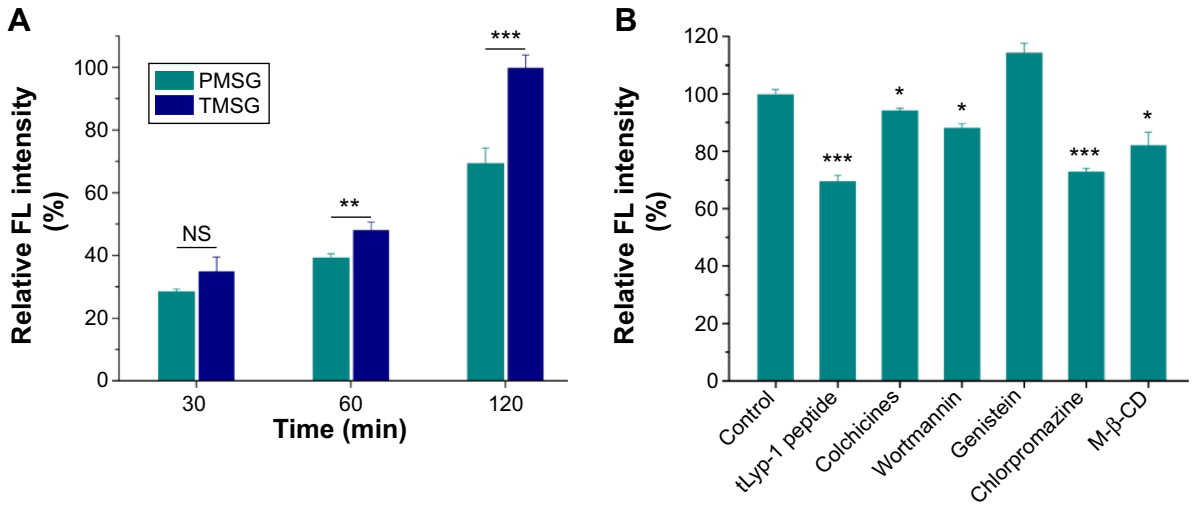

Figure 8 (**A**) Cellular uptake of rhodamine-labeled PMSG or TMSG in MDA-MB-231 cells and then quantization of mean FL intensity by flow cytometry. (**B**) Cellular association of rhodamine-labeled TMSG in the presence of different endocytosis inhibitors in MDA-MB-231 cells.

Notes: The geometric mean of the fluorescence for the cells treated with rhodamine-labeled TMSG without any inhibitors was defined as 100% (n=3). ***$P<0.001$, **$P<0.01$, *$P<0.05$, and NS, not statistically significant.

Abbreviations: FL, fluorescence; PMSG, polyethylene glycol-modified mesoporous silica-coated gold nanorods; TMSG, tLyp-1 peptide-functionalized PMSG; min, minutes; M-β-CD, methyl-β-cyclodextrin; MDA-MB-231cells, MD Anderson-metastatic breast-231 cells.

As consistent with the previous report, silicon or gold nanomaterials in itself show negligible cytotoxicity. We found that TMSG and PMSG exhibited low cytotoxicity (cell survival rate exceeded 90%) even at nanoparticle concentrations as high as 170 μg/mL (Figure 9A). ICG-containing nanoparticles also show good cellular compatibility under dark, and the cell viability could exceed 80% at a concentration of 120 μg/mL (Figure 9B). This result also indicated that ICG, as a FDA-approved clinical imaging agent, presented low dark cytotoxicity.

PTT, as a non-pharmaceutical approach, could kill cancer cells by reaching sufficient hyperthermia under laser irradiation. Therefore, we measured the temperature increase of TMSG solutions in different concentrations under laser exposure (Figure 10A). As clearly shown by the thermography map in Figure 10B, at an irradiation power density of 3 W/cm^2, the temperature rocketed in the first 60 seconds and then gradually reached a plateau within 2 minutes. In sharp contrast, there was no significant temperature change in pure water under the same conditions.

Then, we intuitively confirmed the effectiveness of PTT through co-staining the cells by Calcein-AM and PI to differentiate live (green) and dead (red) cells, respectively. As illustrated in Figure 11, there was no apparent cell death when

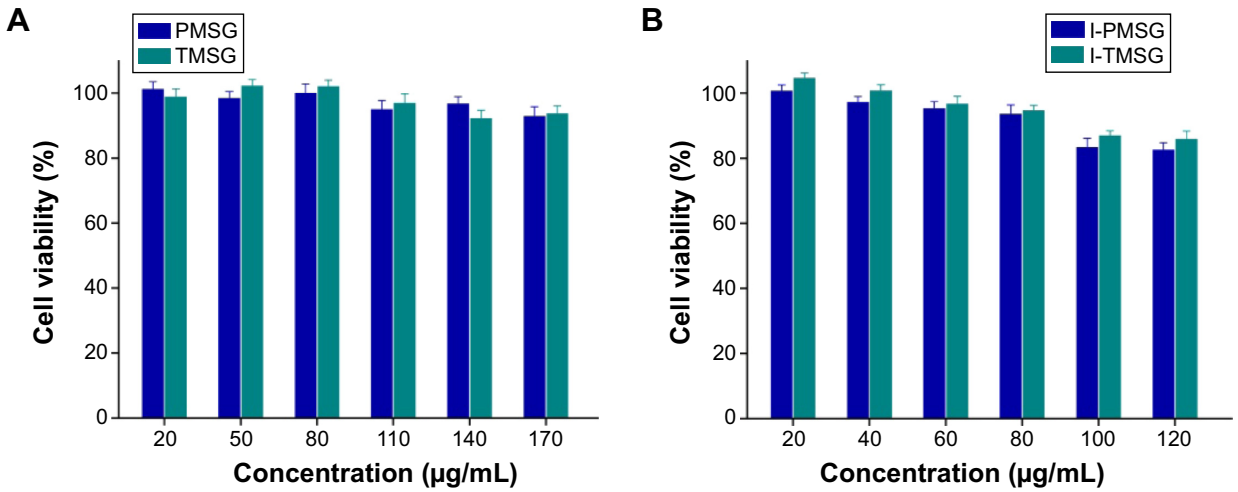

Figure 9 Relative viabilities of MDA-MB-231 cells after being incubated with (**A**) PMSG and TMSG nanoparticles or (**B**) I-PMSG and I-TMSG nanoparticles for 48 hours (n=4).

Abbreviations: PMSG, polyethylene glycol-modified mesoporous silica-coated gold nanorods; TMSG, tLyp-1 peptide-functionalized PMSG; I-PMSG, indocyanine green-containing PMSG; I-TMSG, indocyanine green-containing TMSG; MDA-MB-231cells, MD Anderson-metastatic breast-231 cells.

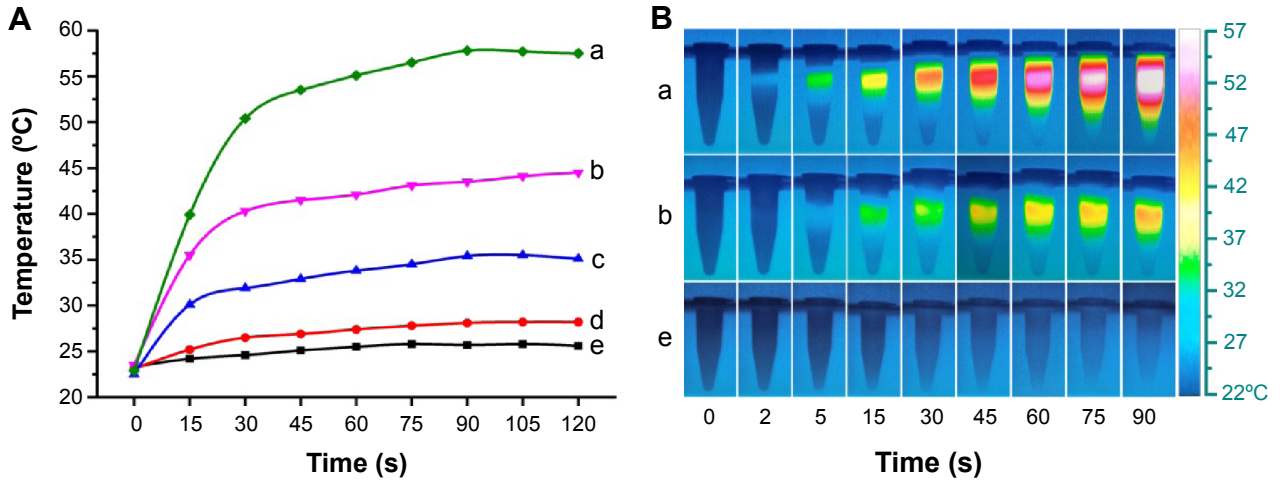

Figure 10 (**A**) Temperature curves and (**B**) thermograph map of different concentrations of TMSG under exposure to a 785-nm laser (3 W/cm^2) over a period of 2 minutes.
Notes: (a) 60 μg/mL, (b) 40 μg/mL, (c) 20 μg/mL, (d) 10 μg/mL, and (e) 0 μg/mL.
Abbreviations: TMSG, tLyp-1 peptide and polyethylene glycol co-modified mesoporous silica-coated gold nanorods; s, seconds.

the cells were treated with either TMSG or laser irradiation, separately. However, massive dead cells in a circular region, which was precisely consistent with the laser spot, were observed when the cells were treated with TMSG plus laser exposure. In addition, compared with PMSG, TMSG appeared to have more powerful photothermal toxicity under the same irradiation dose.

The PTT effects were further confirmed with apoptosis detection by flow cytometry. The tumor cells were treated with PTT and then double-labeled with Annexin V-FITC and PI successively. The results show that PTT treatment significantly induced tumor cell necrosis/late apoptosis (72.9%) compared with control groups (12.7%, Figure 12).

Finally, cell viability test based on CCK-8 assay was performed. Under a 785-nm laser exposure at a density of 3 W/cm^2 for 5 minutes, enhanced photothermal ablation efficacy was observed as the increase in nanoparticle concentrations. More importantly, TMSG showed a significantly stronger cell-killing effect compared with PMSG under the same nanoparticle concentrations ($P<0.01$, Figure 13A), which might be attributed to its robust endocytosis. Besides, PTT effects could be enhanced by increasing laser irradiation time from 30 seconds to 3 minutes. However, relative cell viability was <20% by using a dose of 80 μg/mL of TMSG plus 3 minutes NIR irradiation with power density of 3 W/cm^2 (Figure 13B). All together, these data strongly confirmed that the enhanced photothermal toxicity of tLyp-1 modified TMSG compared with PMSG and further suggested that TMSG nanoparticles could be an effective and promising active-targeting PTT agent.

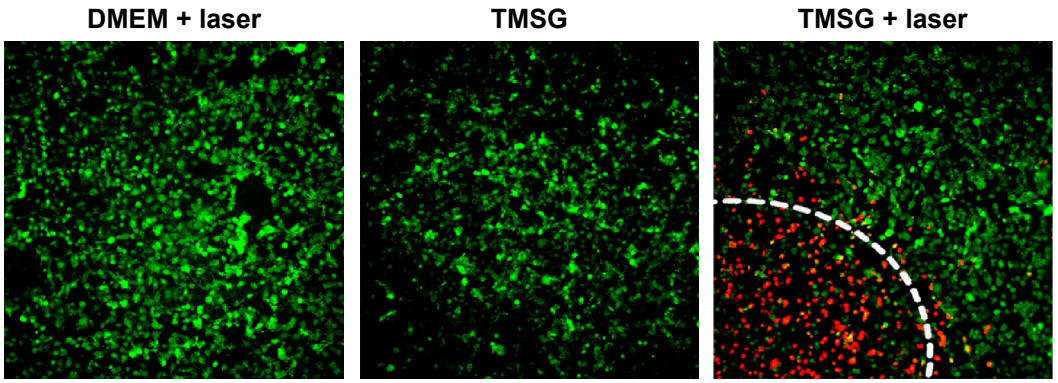

Figure 11 Confocal laser scanning microscope images of Calcein-AM/propidium iodide-costained MDA-MB-231 cells in different treatment conditions.
Notes: The laser irradiated regions are inside a circular area, and the edges are marked with white dashed lines. Viable cells are stained green with Calcein-AM, and dead/later apoptosis cells are floating and eluted or are stained red with propidium iodide.
Abbreviations: DMEM, Dulbecco's Modified Eagle's Medium; TMSG, tLyp-1 peptide and polyethylene glycol comodified mesoporous silica-coated gold nanorods; MDA-MB-231cells, MD Anderson-metastatic breast-231 cells.

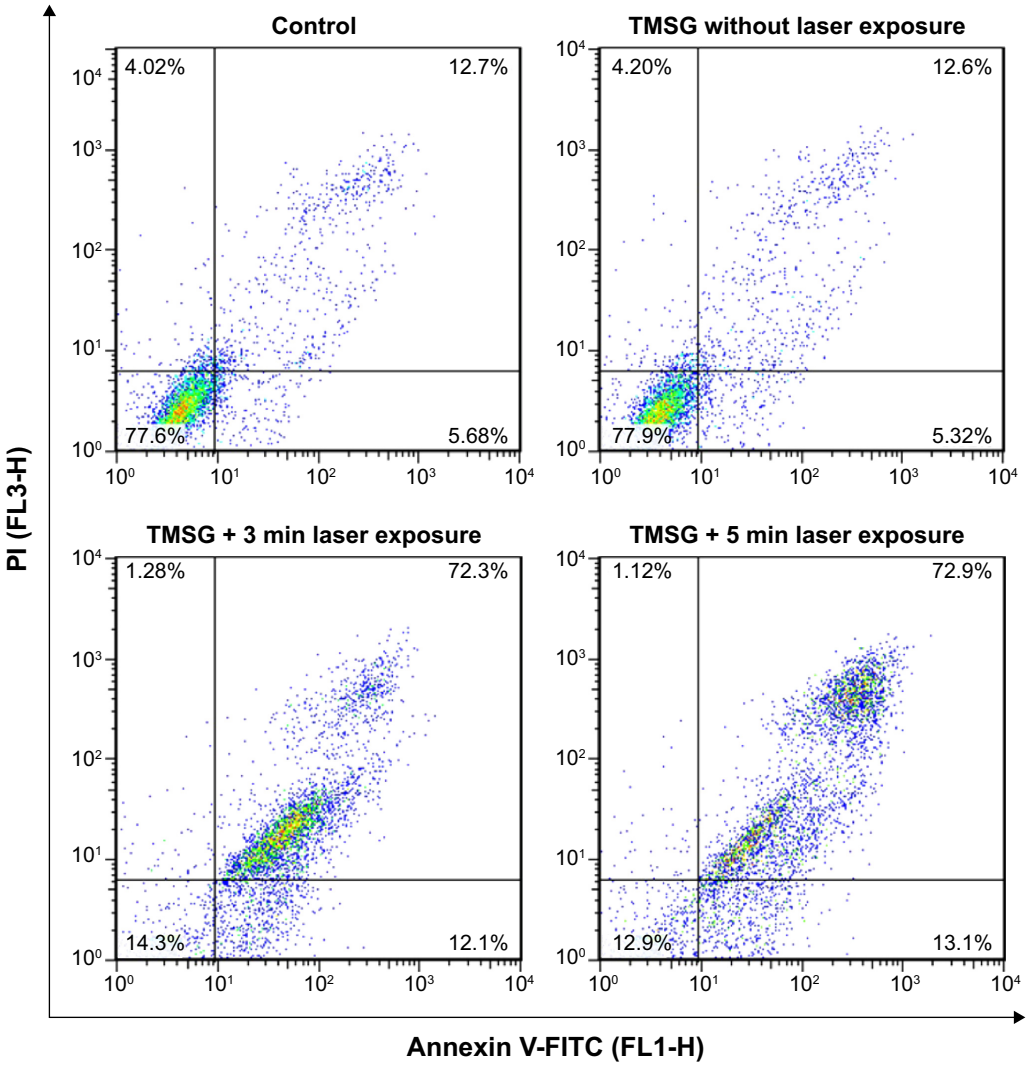

Figure 12 Flow cytometry analysis of MDA-MB-231 cells after photothermal therapy treatments under different treatment conditions.
Notes: The living cell fraction is negative for both Annexin V-FITC and propidium iodide. An earlier stage of apoptosis is linked with positive Annexin V-FITC labeling only. Double-stained cells were considered as necrotic/late apoptotic cells. The concentration of TMSG was 70 μg/mL, and the power density of laser irradiation was 3 W/cm^2.
Abbreviations: TMSG, tLyp-1 peptide and polyethylene glycol-comodified mesoporous silica-coated gold nanorods; PI, propidium iodide; FL, fluorescence; MDA-MB-231 cells, MD Anderson-metastatic breast-231 cells; min, minutes.

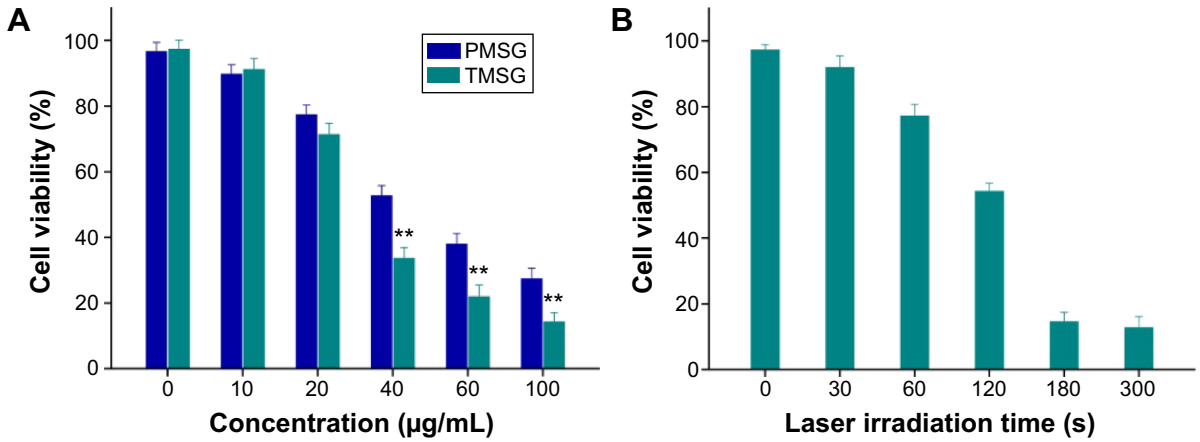

Figure 13 (**A**) Relative viabilities of MDA-MB-231 cells incubated with TMSG or PMSG at different concentrations under exposure to a 785 nm laser at a power density of 3 W/cm^2 for 5 minutes. (**B**) Relative viabilities of MDA-MB-231 cells after TMSG (80 μg/mL) induced photothermal ablation over different laser exposure periods.
Notes: The cell viability values were all normalized to control untreated cells (n=3). $^{**}P<0.01$.
Abbreviations: PMSG, polyethylene glycol-modified mesoporous silica-coated gold nanorods; TMSG, tLyp-1 peptide-functionalized PMSG; s, seconds; MDA-MB-231cells, MD Anderson-metastatic breast-231 cells.

Conclusion

In this study, we have established a type of theranostic nanoagent based on the incorporation of mesoporous silica-encapsulated GNRs, ICG, and target peptides (tLyp-1). The obtained I-TMSG nanomaterials possessed dual functions as targeting fluorescent probes and targeting PTT agents to tumor cells. Therefore, we deemed that such a novel, highly selective, efficient composite-based theranostic nanosystem had huge potential to be translated into cancer diagnosis and treatment.

Acknowledgment

This work was partially supported by National Natural Science Foundation of China (Nos 81341134 and 81202483).

Disclosure

The authors report no conflicts of interest in this work.

References

1. Jaque D, Maestro LM, del Rosal B, et al. Nanoparticles for photothermal therapies. *Nanoscale*. 2014;6(16):9494–9530.
2. Yang K, Zhang SA, Zhang GX, Sun XM, Lee ST, Liu ZA. Graphene in mice: ultrahigh in vivo tumor uptake and efficient photothermal therapy. *Nano Lett*. 2010;10(9):3318–3323.
3. Yuan H, Fales AM, Vo-Dinh T. TAT peptide-functionalized gold nanostars: enhanced intracellular delivery and efficient NIR photothermal therapy using ultralow irradiance. *J Am Chem Soc*. 2012;134(28):11358–11361.
4. Tian Q, Hu J, Zhu Y, et al. Sub-10 nm Fe3O4@Cu2-xS core-shell nanoparticles for dual-modal imaging and photothermal therapy. *J Am Chem Soc*. 2013;135(23):8571–8577.
5. Zha Z, Wang S, Zhang S, et al. Targeted delivery of CuS nanoparticles through ultrasound image-guided microbubble destruction for efficient photothermal therapy. *Nanoscale*. 2013;5(8):3216–3219.
6. Han J, Li J, Jia W, et al. Photothermal therapy of cancer cells using novel hollow gold nanoflowers. *Int J Nanomedicine*. 2014;9(1):517–526.
7. Geng J, Sun C, Liu J, et al. Biocompatible conjugated polymer nanoparticles for efficient photothermal tumor therapy. *Small*. 2015; 11(13):1603–1610.
8. Ma XX, Tao HQ, Yang K, et al. A functionalized graphene oxide-iron oxide nanocomposite for magnetically targeted drug delivery, photothermal therapy, and magnetic resonance imaging. *Nano Res*. 2012;5(3):199–212.
9. Green HN, Crockett SD, Martyshkin DV, et al. A histological evaluation and in vivo assessment of intratumoral near infrared photothermal nanotherapy-induced tumor regression. *Int J Nanomedicine*. 2014;9(1):5093–5102.
10. Kennedy LC, Bickford LR, Lewinski NA, et al. A new era for cancer treatment: gold-nanoparticle-mediated thermal therapies. *Small*. 2011;7(2):169–183.
11. Melancon MP, Lu W, Yang Z, et al. In vitro and in vivo targeting of hollow gold nanoshells directed at epidermal growth factor receptor for photothermal ablation therapy. *Mol Cancer Ther*. 2008;7(6):1730–1739.
12. Liao LD, Tsytsarev V, Delgado-Martínez I, et al. Neurovascular coupling: in vivo optical techniques for functional brain imaging. *Biomed Eng Online*. 2013;12:38.
13. Tsytsarev V, Arakawa H, Borisov S, Pumbo E, Erzurumlu RS, Papkovsky DB. In vivo imaging of brain metabolism activity using a phosphorescent oxygen-sensitive probe. *J Neurosci Methods*. 2013; 216(2):146–151.
14. Yang K, Hu L, Ma X, et al. Multimodal imaging guided photothermal therapy using functionalized graphene nanosheets anchored with magnetic nanoparticles. *Adv Mater*. 2012;24(14):1868–1872.
15. Gobin AM, Lee MH, Halas NJ, James WD, Drezek RA, West JL. Near-infrared resonant nanoshells for combined optical imaging and photothermal cancer therapy. *Nano Lett*. 2007;7(7):1929–1934.
16. Larson TA, Bankson J, Aaron J, Sokolov K. Hybrid plasmonic magnetic nanoparticles as molecular specific agents for MRI/optical imaging and photothermal therapy of cancer cells. *Nanotechnology*. 2007;18(32):325101.
17. Cheng L, Yang K, Li YG, et al. Facile preparation of multifunctional upconversion nanoprobes for multimodal imaging and dual-targeted photothermal therapy. *Angew Chem Int Ed Engl*. 2011; 50(32):7385–7390.
18. Jang B, Park JY, Tung CH, Kim IH, Choi Y. Gold nanorod–photosensitizer complex for near-infrared fluorescence imaging and photodynamic/photothermal therapy in vivo. *ACS Nano*. 2011;5(2):1086–1094.
19. Xie J, Lee S, Chen XY. Nanoparticle-based theranostic agents. *Adv Drug Deliv Rev*. 2010;62(11):1064–1079.
20. Lin X, Xie J, Niu G, et al. Chimeric ferritin nanocages for multiple function loading and multimodal imaging. *Nano Lett*. 2011;11(2): 814–819.
21. Abeylath SC, Ganta S, Iyer AK, Amiji M. Combinatorial-designed multifunctional polymeric nanosystems for tumor-targeted therapeutic delivery. *Acc Chem Res*. 2011;44(10):1009–1017.
22. Yi XM, Wang FL, Qin WJ, Yang XJ, Yuan JL. Near-infrared fluorescent probes in cancer imaging and therapy: an emerging field. *Int J Nanomedicine*. 2014;9(1):1347–1365.
23. Lammers T, Aime S, Hennink WE, Storm G, Kiessling F. Theranostic nanomedicine. *Acc Chem Res*. 2011;44(10):1029–1038.
24. Chen Q, Wang C, Cheng L, He WW, Cheng Z, Liu Z. Protein modified upconversion nanoparticles for imaging-guided combined photothermal and photodynamic therapy. *Biomaterials*. 2014;35(9):2915–2923.
25. Zhang L, Gao S, Zhang F, Yang K, Ma Q, Zhu L. Activatable hyaluronic acid nanoparticle as a theranostic agent for optical/photoacoustic image-guided photothermal therapy. *ACS Nano*. 2014;8(12): 12250–12258.
26. Fan Z, Senapati D, Singh AK, Ray PC. Theranostic magnetic core-plasmonic shell star shape nanoparticle for the isolation of targeted rare tumor cells from whole blood, fluorescence imaging, and photothermal destruction of cancer. *Mol Pharm*. 2013;10(3):857–866.
27. Topete A, Alatorre-Meda M, Iglesias P, et al. Fluorescent drug-loaded, polymeric-based, branched gold nanoshells for localized multimodal therapy and imaging of tumoral cells. *ACS Nano*. 2014; 8(3):2725–2738.
28. Nikoobakht B, El-Sayed MA. Preparation and growth mechanism of gold nanorods (NRs) using seed-mediated growth method. *Chem Mater*. 2003;15(10):1957–1962.
29. Huang XH, El-Sayed IH, Qian W, El-Sayed MA. Cancer cell imaging and photothermal therapy in the near-infrared region by using gold nanorods. *J Am Chem Soc*. 2006;128(6):2115–2120.
30. Guerrero AR, Hassan N, Escobar CA, Albericio F, Kogan MJ, Araya E. Gold nanoparticles for photothermally controlled drug release. *Nanomedicine*. 2014;9(13):2023–2039.
31. Niidome T, Yamagata M, Okamoto Y, et al. PEG-modified gold nanorods with a stealth character for in vivo applications. *J Control Release*. 2006;114(3):343–347.
32. Cabada TF, de Pablo CSL, Serrano AM, Guerrero FD, Olmedo JJS, Gomez MR. Induction of cell death in a glioblastoma line by hyperthermic therapy based on gold nanorods. *Int J Nanomedicine*. 2012;7:1511–1523.
33. Alkilany AM, Boulos SP, Lohse SE, Thompson LB, Murphy CJ. Homing peptide-conjugated gold nanorods: the effect of amino acid sequence display on nanorod uptake and cellular proliferation. *Bioconjug Chem*. 2014;25(6):1162–1171.
34. Hu XG, Gao XH. Multilayer coating of gold nanorods for combined stability and biocompatibility. *Phys Chem Chem Phys*. 2011; 13(21):10028–10035.

35. Zhu XM, Fang C, Jia H, et al. Cellular uptake behaviour, photothermal therapy performance, and cytotoxicity of gold nanorods with various coatings. *Nanoscale*. 2014;6(19):11462–11472.
36. Chen HJ, Shao L, Li Q, Wang JF. Gold nanorods and their plasmonic properties. *Chem Soc Rev*. 2013;42(7):2679–2724.
37. Zhang Z, Wang J, Nie X, et al. Near infrared laser-induced targeted cancer therapy using thermoresponsive polymer encapsulated gold nanorods. *J Am Chem Soc*. 2014;136(20):7317–7326.
38. Liu XS, Huang N, Li H, Wang HB, Jin Q, Ji J. Multidentate polyethylene glycol modified gold nanorods for in vivo near-infrared photothermal cancer therapy. *ACS Appl Mater Interfaces*. 2014;6(8):5657–5668.
39. Zhang L, Xia K, Bai YY, et al. Synthesis of gold nanorods and their functionalization with bovine serum albumin for optical hyperthermia. *J Biomed Nanotechnol*. 2014;10(8):1440–1449.
40. Li XJ, Takashima M, Yuba E, Harada A, Kono K. PEGylated PAMAM dendrimer-doxorubicin conjugate-hybridized gold nanorod for combined photothermal-chemotherapy. *Biomaterials*. 2014;35(24):6576–6584.
41. Duan R, Zhou Z, Su G, et al. Chitosan-coated gold nanorods for cancer therapy combining chemical and photothermal effects. *Macromol Biosci*. 2014;14(8):1160–1169.
42. Xu B, Ju Y, Cui Y, et al. tLyP-1-conjugated Au-Nanorod@SiO_2 core-shell nanoparticles for tumor targeted drug delivery and photothermal therapy. *Langmuir*. 2014;30(26):7789–7797.
43. Wang D, Xu Z, Yu H, et al. Treatment of metastatic breast cancer by combination of chemotherapy and photothermal ablation using doxorubicin-loaded DNA wrapped gold nanorods. *Biomaterials*. 2014;35(29):8374–8384.
44. Roth L, Agemy L, Kotamraju VR, et al. Transtumoral targeting enabled by a novel neuropilin-binding peptide. *Oncogene*. 2012;31(33):3754–3763.
45. Soker S, Takashima S, Miao HQ, Neufeld G, Klagsbrun M. Neuropilin-1 is expressed by endothelial and tumor cells as an isoform-specific receptor for vascular endothelial growth factor. *Cell*. 1998;92(6):735–745.
46. Ntziachristos V, Bremer C, Weissleder R. Fluorescence imaging with near-infrared light: new technological advances that enable in vivo molecular imaging. *Eur Radiol*. 2003;13(1):195–208.
47. Busbee BD, Obare SO, Murphy CJ. An improved synthesis of high-aspect-ratio gold nanorods. *Adv Mater*. 2003;15(5):414–416.
48. Huang CC, Huang CH, Kuo IT, Chau LK, Yang TS. Synthesis of silica-coated gold nanorod as Raman tags by modulating cetyltrimethylammonium bromide concentration. *Colloid Surf A Physicochem Eng*. 2012;409:61–68.
49. Zheng X, Xing D, Zhou F, Wu B, Chen WR. Indocyanine green-containing nanostructure as near infrared dual-functional targeting probes for optical imaging and photothermal therapy. *Mol Pharm*. 2011;8(2):447–456.
50. Hu Q, Gao X, Gu G, et al. Glioma therapy using tumor homing and penetrating peptide-functionalized PEG-PLA nanoparticles loaded with paclitaxel. *Biomaterials*. 2013;34(22):5640–5650.
51. Yang ZZ, Li JQ, Wang ZZ, Dong DW, Qi XR. Tumor-targeting dual peptides-modified cationic liposomes for delivery of siRNA and docetaxel to gliomas. *Biomaterials*. 2014;35(19):5226–5239.

Supplementary materials

A detailed description of the characterization of the nanoparticles

The qualitative assay of tLyp-1 bound on the TMSG was determined by BCA assay. Briefly, the BCA working solution was prepared by mixing the reagent A with reagent B (reagent A:B=50:1, v/v) for further use. Then, 20 μL of TMSG nanoparticles were added into 96-well plate, followed by incubation with 200 μL of BCA working solution. After 30 minutes at 37°C, the assay was carried out at 570 nm by using a microplate reader (Synergy TM2; BioTek Instruments Inc., USA) and PMSG and MSG acted as control.

The drying nanoparticles samples were also subjected to XPS analysis via an XPS system (ESCALAB 250Xi; Thermo Fisher Scientific, Waltham, MA, USA) to determine the surface composition. Moreover, the samples were subjected to TGA analysis under a controlled atmosphere of nitrogen from 90°C up to 690°C at a constant heating rate of 10°C/min using TGA system (SDT-2960; TA Instruments, USA).

Cell lines and culture conditions

MDA-MB-231 cell line was obtained from the Cell Institute of Chinese Academy of Sciences (Shanghai, People's Republic of China) and then cultured in DMEM medium supplemented with 10% (v/v) fetal bovine serum, 100 IU/mL penicillin, and 100 μg/mL streptomycin sulfate at 37°C in 5% CO_2.